Applied Catalysis B: Environment and Energy 354 (2024) 124143

Contents lists available at ScienceDirect

Applied Catalysis B: Environment and Energy

journal homepage: www.elsevier.com/locate/apcatb

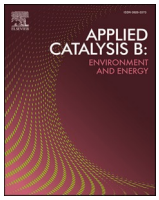

Spin-cross interface-inducing ultra-high catalytic activity in Co$(OH)_xP_y$-MXene toward alkali-free liquid hydrogen generation

Yanyan Liu [a,b,d], Huanhuan Zhang [a,b,c], Jingjing Zhou [a], Shuyan Guan [b,c], Ruofan Shen [b], Wenbo Zhang [a], Xia Sheng [a], Lixia Wang [a], Xianji Guo [b], Xianli Wu [b], Jianchun Jiang [d], Baozhong Liu [c,*], Yongfeng Wang [e,*], Baojun Li [b,c,f,**]

[a] College of Science, Henan Agricultural University, 95 Wenhua Road, Zhengzhou 450002, PR China
[b] College of Chemistry, Zhengzhou University, 100 Science Road, Zhengzhou 450001, PR China
[c] College of Chemistry and Chemical Engineering, Henan Polytechnic University, 2001 Century Avenue, Jiaozuo 454000, PR China
[d] Institute of Chemical Industry of Forest Products, CAF, National Engineering Lab for Biomass Chemical Utilization, Key and Open Lab on Forest Chemical Engineering, SFA, 16 Suojinwucun, Nanjing 210042, PR China
[e] Center for Carbon-based Electronics and Key Laboratory for the Physics and Chemistry of Nanodevices, Department of Electronics, Peking University, Beijing 100871, PR China
[f] Department of Chemistry, Tsinghua University, Beijing 100084, PR China

ARTICLE INFO

Keywords:
Bimolecular activation
Cobalt catalysts
MXene
P-inducing
Spin-cross interface

ABSTRACT

Proclaiming the interfacial active sites of non-noble metals on supported catalysts is a paramount topic. Herein, a spin-cross interface ($Co(OH)_xP_y$ (x/y=3.2)) in the intimate region between $Co(OH)_2$ and CoP is designed by *in situ* hydroxylation and P-inducing strategy. An ultra-high catalytic hydrogen generation activity with a turnover frequency of 1640 min^{-1} is achieved for hydrolysis of ammonia borane (NH_3BH_3). Both experimental observations and computational simulations reveal that the spin-cross interface dramatically reduces the energy barriers for the dissociation of reactant molecules (NH_3BH_3 and H_2O) to expedite the catalytic activity. The coexistence of active interface and MXene create the ensembles of Co atoms coordinated by OH and P. The construction of active sites of $Co(OH)_xP_y$ simultaneously boosts the adsorption and dissociation of H_2O and NH_3BH_3 molecules. This research provides new paradigm for the rational design of spin-induced catalysts in the future energy system depending on the activation of multi-molecules.

1. Introduction

Although noble metals possess excellent activity in catalytic reactions because of their unique atomic orbitals and electronic properties, rocket cost and earth-limited availability severely impede large-scale applications in the next-generation industry [1,2]. Non-noble metal-based catalysts are featured with abundant reserves and price advantages have been captured by extensive attention [3]. Therefore, the development of non-noble metal-based catalysts with noble metal-like behavior is beneficial to satisfy the profound demands of the catalysis for energy conversion and storage [4]. The spin state of transition metal atoms can be modified between low and high spin state, producing less/more unpaired electrons at its 3d-orbit in the presence of a magnetic/coordination field. This phenomenon can induce moderate adsorption free energy of some species to reduce activation barriers for boosting catalytic activity [5]. The accurate regulation of the electronic states of active sites and energy band structure in active matter or phase expedites the hydrogen generation on non-noble metal-based catalysts. However, the excavation of practicable strategies to boost the catalytic activity of non-noble metal-based catalysts comparable to those of noble metal-based counterparts is scientifically challenging in the field of industrial catalysis. Therefore, innovative design of active sites based on spin regulation in non-noble metal-based catalysts is imperative for the promotion of the catalytic activity toward hydrogen generation [6,7].

Understanding the catalytic role of spin and modulating the spin state of active sites is of profound fundamental guidance for spin catalysis [8]. The electronic structure and spin state of catalytic sites depends on the changes in the surrounding chemical environment of

* Corresponding authors.
** Corresponding author at: College of Chemistry, Zhengzhou University, 100 Science Road, Zhengzhou 450001, PR China.
E-mail addresses: HPUliuking@163.com (B. Liu), yongfengwang@pku.edu.cn (Y. Wang), lbjfcl@zzu.edu.cn (B. Li).

https://doi.org/10.1016/j.apcatb.2024.124143
Received 2 January 2024; Received in revised form 23 April 2024; Accepted 29 April 2024
Available online 30 April 2024

transition metal atoms [9]. Supported metal catalysts are one of the most commonly employed catalysts in the catalysis field because of the formation of the metal-support interface caused by the catalytic metal species deposited onto supports or decorated by supports [10–12]. The balance of positive dispersion and excellent activity is an imminent challenge during the design and manufacture of supported catalysts [13]. Due to the advantages of excellent metallic conductivity, favorable hydrophilicity, adjustable layered structure and surface composition, MXenes hold the promise as elemental matter for the application in energy catalysis [14,15]. The coupling effect via coordination, electrostatic, Van der Waals interaction between MXene and metal ions induces active sites or nucleation sites for the synthesis of MXene-based composites through adsorbing and anchoring [16]. In the construction of MXene-based catalysts, the insufficiency of active sites with high-efficiency restricted by the weak ability to adsorb and activate reactant molecules of MXene leads to a sluggish kinetics [17]. The fabrication of interface active sites with different spin state on MXene is the bottleneck of the regulation of electronic structure and the expedition of the intrinsic activity of non-noble metal-based catalysts.

Alkali, such as, sodium hydroxide (NaOH) as a co-catalyst plays an important role in the improvement of the hydrogen generation. NaOH works only the hydroxyl in near the interface. Namely, a consumption occurs when high concentration NaOH or other alkaline substances used in the process of hydrogen generation. Much literature has been reported that NaOH displays positive effect on the enhancement of hydrogen generation from NH_3BH_3 because of the role of co-catalyst of NaOH [1,18–20]. The results confirm that the obtained catalysts lack of the function like sodium hydroxide function as a cocatalyst from another point of view. The usage of NaOH has some damage: the generated ammonia is negative for the practice application; the other is the corrosion of the reactor because of the high concentration of alkali. Therefore, it is necessary to research the other active substance to substitute for NaOH to boost catalytic activity under the condition without alkali. The construction of active hydroxyl near the active sites has the ability to replace NaOH. Surface hydroxylation of active phases endows the catalysts with hydrophilicity and surface properties involves surface charge fluctuations, interface charge transfer, electronic structure configuration and so on [21,22]. The local space charge separation, high-efficiency active sites for adsorption, effective conversion of reactive oxygen species caused by surface hydroxylation accelerates the activity of solid composite catalysts toward photo-, electro-, and thermo-catalysis [23–25]. The flexible regulation of electronic structure and surface chemistry by surface hydroxylation favors the catalytic activity [26,27]. Therefore, specific fabrication strategies and operation platforms are necessary for rational regulation of atomic and electronic structures of catalysts to optimize the catalytic reaction.

The electronic spin polarization is able to increase the overlap-integral between catalysts and precursor/intermediate/product species to enhance charge transfer, thus boosting the binding energy and potentially the reaction pathway [5,9]. The inadequate design of catalysts based on electron spin is single spin state. Transition-metal phosphides (TMPs) obtained through P-inducing strategy as active matters or precursors for advanced catalysts have attracted extensive attention in the field of energy catalysis because of their unique orbital electron configurations and abundance in nature [28–30]. Phosphorus (P) element endows lone-pair electrons in 3p orbitals and vacant 3d orbitals, induce local charge density and accommodate the surface charge state, thus igniting the catalytic activity of phosphides [31]. The surface hydroxylation and P-inducing strategy simultaneously modulates the electronic structure of active species and then boosts the intrinsic catalytic activity. The construction of the spin-induced active sites on the surface of MXene through surface hydroxylation and P-inducing strategy to enhance the intrinsic catalytic activity of catalysts still remains challenges. Therefore, the rational design of the spin-induced active sites on MXene through the introduction of OH and P is necessary to further heighten the catalytic activity of non-noble metal-based catalysts for hydrogen generation.

Herein, a spin-cross interface is designed in the intimate region between $Co(OH)_2$ and CoP through *in situ* hydroxylation and P-inducing strategy (the spin-cross interface is referred to the interface with two spin states on both sides of interface). The different coordination modes in $Co(OH)_2$ and CoP induce two spin states of Co. The spin-cross interface containing two different Co spin states generates the corresponding bifunctional active sites of $Co(OH)_xP_y$. The optimal catalyst attains a top-ranked *TOF* of 1640 min^{-1} among the P-based catalysts in alkaline additives-free hydrolysis of NH_3BH_3 because of the construction of the spin-cross interface. The superior catalytic activity remains without deteriorative decrease after long-time usage. The interfacial $Co(OH)_xP_y$ is responsible for the dissociation of reactant molecules ($Co(OH)_2$ activate H_2O, CoP activate NH_3BH_3) and the enhancement of intrinsic catalytic activity. Density functional theory (DFT) calculations reveal that the spin-cross interface extremely optimizes the adsorption energies through reducing the energy barriers for dissociation of NH_3BH_3 and H_2O molecules. This research proffers universal guidance in reinforcing the performances of non-noble metal-based catalysts for energy chemistry and industry.

2. Experimental section

2.1. Reagents and chemicals

All chemical reagents were purchased from commercial suppliers and used without further purification. Titanium hydride (TiH_2, −325 mesh, Shanghai Aladdin, Co., Ltd., 99%), aluminum (Al, particle size<40 μm), and graphite (particle size <48μm) with 99 wt%. hydrofluoric acid (HF, Alfa Aesar 49%). Sodium hypophosphite (NaH_2PO_2, Shanghai Macklin Biochemical Co., Ltd., AR, 99%), ammonia borane (NH_3BH_3, Energy Chemical Reagent Co., Ltd., 98%), cobalt nitrate hexahydrate ($Co(NO_3)_2{\cdot}6\ H_2O$, Shanghai Aladdin, Co., Ltd., AR, 99%), Hexamethylenetetramine (HMT, $C_6H_{12}N_4$, shanghai PERFEMIKER Co., Ltd.,), Trisodium citrate dihydrate ($C_6H_5Na_3O_7{\cdot}2\ H_2O$, Sinopharm Chemical Reagent Co., Ltd., AR), ethanol solution (Sinopharm Chemical Reagent Co., Ltd., AR) and distilled water were used as received.

2.2. Preparation of catalysts

Synthesis of Co-(OH)$_2$/MXene. First, MXene was successfully fabricated according to the previous report and the corresponding details were shown in Supporting Information [32]. In detail, the obtained MXene (Ti_3C_2, 40 mg) was added to the deionized water (20 mL) by stirring and ultrasonic dispersion for 2 h at a time interval of 30 min. Subsequently, $Co(NO_3)_2{\cdot}6\ H_2O$ (1000 mg) was dissolved in deionized water (10 mL) to generate homogeneous solution. Next, hexamethylenetetramine (HMT, $C_6H_{12}N_4$, 500 mg) and trisodium citrate dihydrate ($C_6H_5Na_3O_7{\cdot}2\ H_2O$, 100 mg) were put into deionized water (20 mL) to form a unform solution. The above-mentioned solution was added to the cobalt ion solution with a stirring for 30 min. Then the MXene suspension was put into the uniform solution to keep stirring for 30 min. The as-prepared solution was transferred into a three-necked flask and given an operation of in situ hydroxylation at 90 °C for 9 h under N_2 flow. After the reaction system naturally cooled to room temperature, Co$(OH)_2$/MXene was collected through the centrifugation conduction (distilled water and ethanol several times) following by a drying overnight (> 12 h) at 30 °C in vacuum oven.

Synthesis of Co(OH)$_2$-CoP/MXene. Certain amounts of sodium hypophosphite (NaH_2PO_2) and $Co(OH)_2$/MXene were placed on the upstream and downstream sides of the tube furnace (mass ratio: 10/1), respectively. Then a heating treatment was implemented at 300 °C with a heating rate of 5 °C·min^{-1} to keep for 2 h under Ar atmosphere to fabricate $Co(OH)_2$-CoP/MXene. Additionally, the CoP, Co_3O_4, Co_3O_4-P and Co_3O_4-P/MXene were also prepared under similar procedures. Namely, the CoP was obtained through direct P-inducing treatment of

$Co(OH)_2$. Co_3O_4-P and Co_3O_4-P/MXene were achieved through oxidation and corresponding P-inducing treatment of $Co(OH)_2$ (with MXene or without). Co_3O_4 sample was harvested through direct oxidation of $Co(OH)_2$ (no MXene).

2.3. Hydrolysis of NH_3BH_3 and $NaBH_4$

Catalytic experiments of as-prepared catalysts for NH_3BH_3 hydrolysis were carried out via simple water-displacement method. Details are shown in Supporting Information.

2.4. Characterization

The technologies of X-ray powder diffraction (XRD), scanning electron microscope (SEM), transmission electron microscope (TEM). X-ray photoelectron spectroscopy (XPS), Raman spectra, inductively coupled plasma optical emission spectrometry (ICP-OES) are applied in this research. The detailed information is as shown in Supporting Information.

2.5. Computational details

We have employed the first-principles to perform all spin-polarization DFT calculations within the generalized gradient approximation (GGA) using the Perdew-Burke-Ernzerhof (PBE) functional. We have chosen the projected augmented wave (PAW) potentials to describe the ionic cores and take valence electrons into account using a plane wave basis set with a kinetic energy cutoff of 450 eV. Partial occupancy of the Kohn−Sham orbitals were allowed using the Gaussian smearing method and a width of 0.05 eV. The electronic energy was considered self-consistent when the energy change was smaller than 10^{-5} eV. A geometry optimization was considered convergent when the energy change was smaller than 0.05 eV·Å^{-1}. In our structure, the U correction is used for Co and Ti atoms. The vacuum spacing in a direction perpendicular to the plane of the structure is 20 Å for the surfaces. The Brillouin zone integration is performed using 2×2×1 Monkhorst-Pack k-point sampling for a structure. Finally, the adsorption energies (E_{ads}) were calculated as $E_{ads}=E_{ad/sub}-E_{ad}-E_{sub}$, where $E_{ad/sub}$, E_{ad}, and E_{sub} are the total energies of the optimized adsorbate/substrate system, the adsorbate in the structure, and the clean substrate, respectively. The free energy was calculated using the equation:

$$G=E_{ads}+E_{ZPE}-TS$$

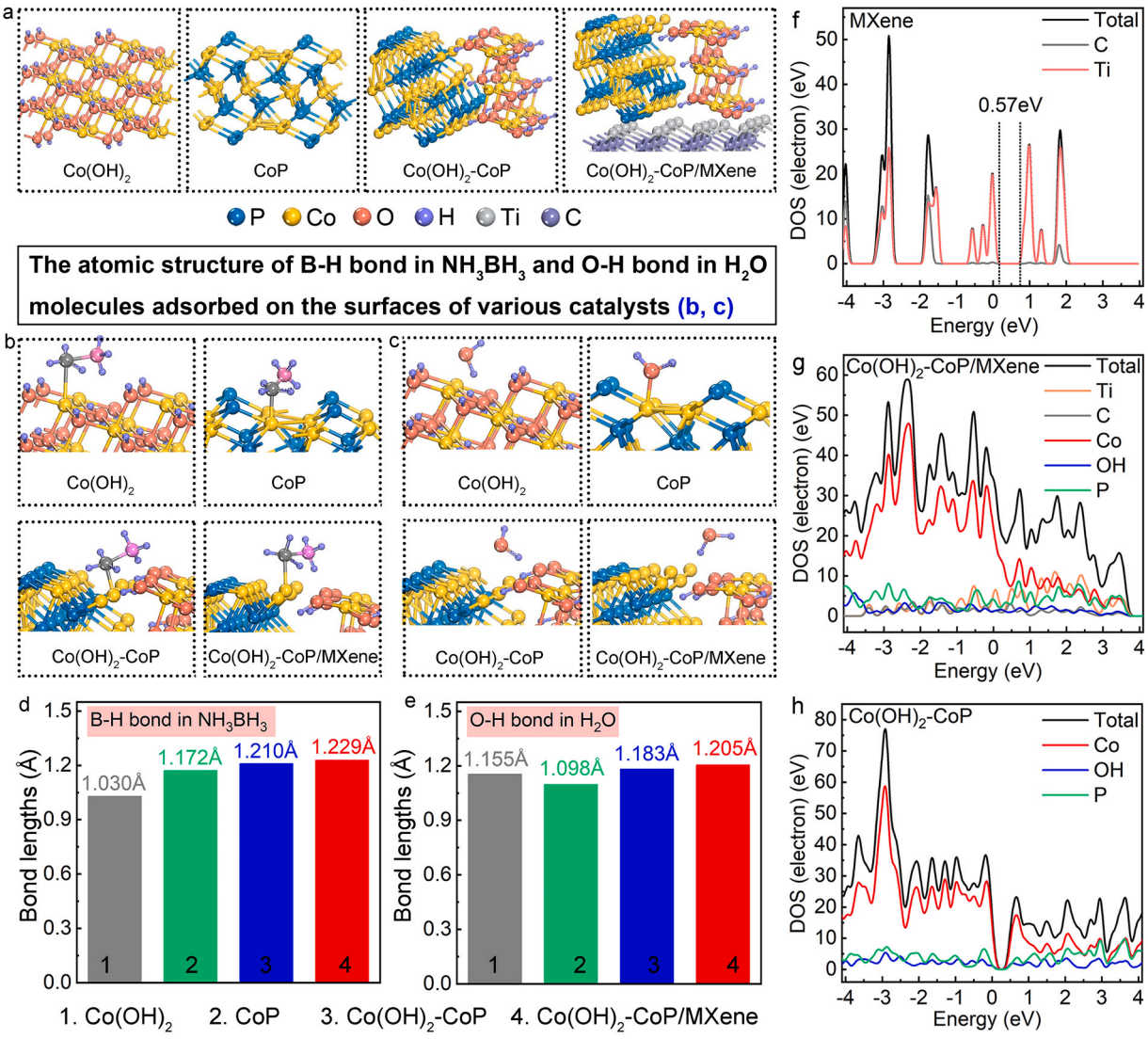

Fig. 1. (a) Optimized atomic structures of various catalysts. (b-e) Atomic models of NH_3BH_3 and H_2O molecules adsorbed on catalyst surfaces and the corresponding B−H, O−H bond lengths in NH_3BH_3 and H_2O molecules. (f-h) The total and partial elements DOS of MXene, $Co(OH)_2$-CoP/MXene and $Co(OH)_2$-CoP.

where G, E_{ads}, E_{ZPE} and TS are the free energy, total energy from DFT calculations, zero point energy and entropic contributions, respectively.

Generally, k_0 refers to the reaction constant (TOF=min^{-1}), E_a is activation energy, R is the ideal gas constant (8.314 $J{\cdot}K^{-1}{\cdot}mol^{-1}$), A represents the pre-exponential factor, and T is the reaction temperature.

3. Results and discussion

3.1. Calculation on theory-guided

Firstly, DFT calculations are manipulated to probe the precise effect of the spin-cross interface ($Co(OH)_2$ and CoP) on enhancing the catalytic performance of $Co(OH)_2$-CoP/MXene. Fig. 1a is the atomic structure model of various catalysts ($Co(OH)_2$-CoP/MXene, $Co(OH)_2$-CoP, $Co(OH)_2$, CoP) in this calculation system. Figs. 1b and 1c accommodate the optimized models of NH_3BH_3 and H_2O molecules adsorbed on various structure surfaces. Bond lengths of B−H and O−H in NH_3BH_3 and H_2O molecules are vital for the release of hydrogen. The specific results of the bond lengths of B−H and O−H are exhibited in Figs. 1d and 1e, respectively. The bond length of B−H in NH_3BH_3 on $Co(OH)_2$-CoP/MXene (1.229 Å) is higher than that on $Co(OH)_2$-CoP (1.210 Å), CoP (1.172 Å) and $Co(OH)_2$ (1.030 Å) (Fig. 1d). The results clarify that the weaker bond energy of B−H bond make NH_3BH_3 molecules have predominance of dissociation on $Co(OH)_2$-CoP/MXene. Coincidentally, the bond length of O–H on $Co(OH)_2$-CoP/MXene (1.205 Å) has the advantage over $Co(OH)_2$-CoP (1.193 Å) of CoP (1.098 Å) and $Co(OH)_2$ (1.155 Å) (Fig. 1e). The intuitive evidence points to that H_2O molecule is more easily dissociated on $Co(OH)_2$-CoP/MXene. The weak bond energy of B–H (O–H) bonds in NH_3BH_3 (H_2O) molecule after adsorption on the surface of $Co(OH)_2$-CoP/MXene are conducive to release the H radical and boost the generation of hydrogen [33]. The existence of the spin-cross interface of $Co(OH)_2$ and CoP on MXene has an optimistic effect on weakening the bond energies of B–H and O–H bonds in the reaction molecule. The construction of spin-cross interface ensures a maximum exposure of active sites and effectively enhanced the catalytic activity [34]. The electronic density of states (DOS) is calculated to analyze the electronic structure of various structures. The DOS of pristine MXene in Fig. 1f presents a band-gap of 0.57 eV [35]. The band-gap in the same position is invisible after the introduction of spin-cross interface ($Co(OH)_2$ and CoP) on MXene (Fig. 1g). The above results verify that the active ingredient is introduced in catalyst. The DOS of Co $(OH)_2$-CoP/MXene near the Fermi level compared with MXene and Co $(OH)_2$-CoP is apparently enhanced. This phenomenon substantiates that higher charge carrier density and favorable charge transfer exist on the surface of $Co(OH)_2$-CoP/MXene in the catalytic process of NH_3BH_3 hydrolysis [36–38]. These results unveil the synergistic coupling of spin-cross interface in $Co(OH)_2$-CoP/MXene for excellent catalytic activity (Fig. 1f-h). The DOS of $Co(OH)_2$ and CoP are supplied and the results define that the existence of Co, OH, and P in corresponding catalysts (Fig. S1). The above DFT calculations expound that spin-cross interface in $Co(OH)_2$-CoP/MXene dominates key factor optimizing the dissociation ability to NH_3BH_3 and H_2O molecules toward hydrogen generation.

3.2. Characterization of surface structure

The schematic illustration of the synthesis of $Co(OH)_2$-CoP/MXene is displayed in Fig. 2a. The MXene is received through the etching of MAX (Ti_3AlC_2) with HF to remove the Al layers and following an alkaline treatment (alk-Ti_3C_2) [32]. From the XRD results in Fig. S2, the peak at 39° (104 plane) in MXene disappeared and synchronously the peak of 8.8° has a downward tendency compared with Ti_3AlC_2 (9.5°). The results corroborate the layer spacing exists in MXene and confirm the successful etching of MXene. The single-active surface of $Co(OH)_2$ is

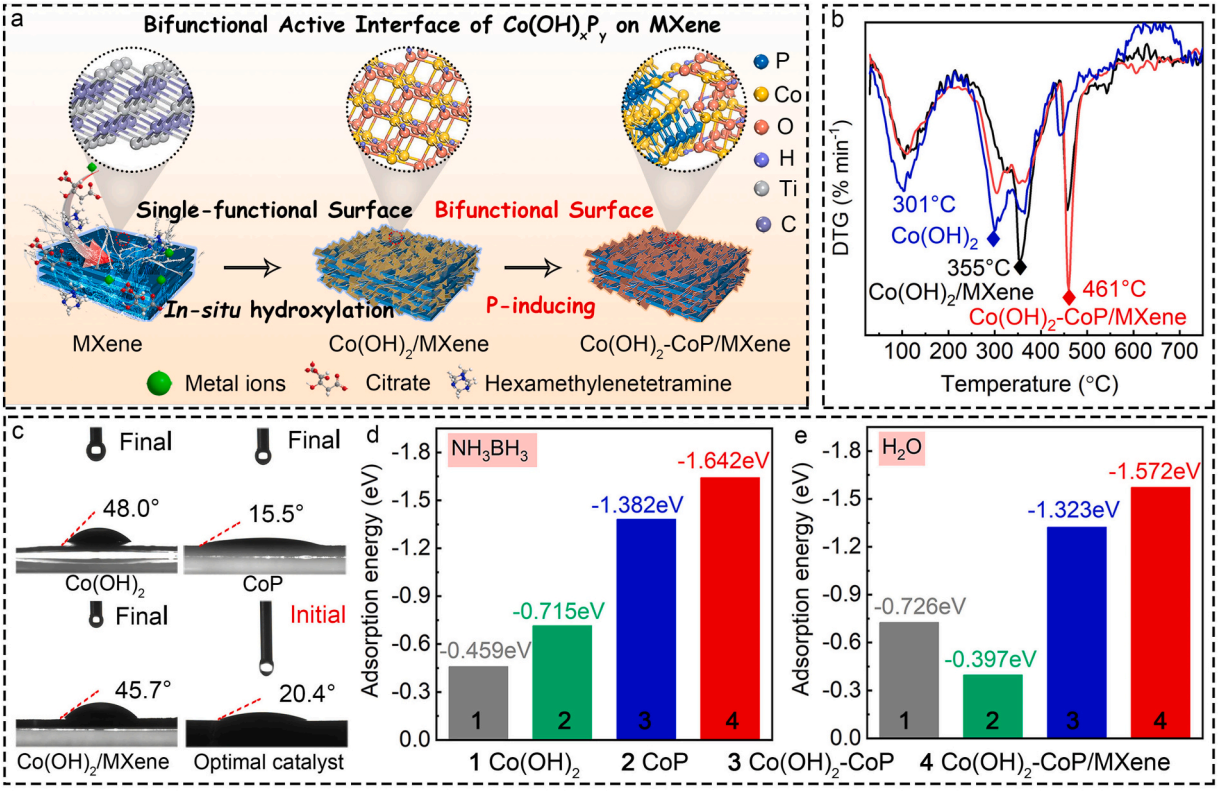

Fig. 2. (a) Diagram of structural evolution process of $Co(OH)_2$-CoP/MXene. (b) The DTG curves of $Co(OH)_2$, $Co(OH)_2$/MXene and $Co(OH)_2$-CoP/MXene tested in Ar atmosphere. (c) Water contact angles and (d, e) adsorption energies of NH_3BH_3 and H_2O molecules on surfaces of $Co(OH)_2$, CoP, $Co(OH)_2$/MXene and $Co(OH)_2$-CoP/MXene catalysts.

successfully constructed on MXene ($Co(OH)_2$/MXene) via *in situ* hydroxylation under the protection of N_2 atmosphere. The spin-cross interface in the intimate region between $Co(OH)_2$ and CoP on MXene ($Co(OH)_2$-CoP/MXene) is achieved through the P-inducing strategy, namely, a transformation process of $Co(OH)_2$/MXene precursor via the chemical vapor deposition induced by PH_3 gas.

The key protective role of MXene during the evolution of bifunctional active surface is as validated by derivative thermogravimetry (DTG) curves of $Co(OH)_2$/MXene and $Co(OH)_2$-CoP/MXene. The manipulation is carried out in Ar atmosphere through the thermogravimetric analysis (TGA). From the results in Fig. 2b, the decomposition temperature of $Co(OH)_2$ increases from 301 ℃ to 355 ℃ after the introduction of MXene. After the operation of P-inducing strategy on $Co(OH)_2$/MXene, the decomposition temperature of $Co(OH)_2$-CoP/MXene increases up to 461 ℃. The existence of MXene decreases the decomposition temperature of $Co(OH)_2$ and prevents its rapid pyrolysis. The results corroborate that MXene stabilizes $Co(OH)_2$ and makes an attribution for the formation of spin-cross interface of $Co(OH)_2$ and CoP. The experiments of contact angle (CA) are conducted to reveal the hydrophilicity/hydrophobicity of catalysts. From Fig. 2c, the CA of $Co(OH)_2$ (48.0°), $Co(OH)_2$/MXene (45.7°), and CoP (15.5°) has a downward tendency. The phenomenon confirms that the introduction of P atom and MXene increase the hydrophilic properties of catalyst and favor the accessibility of reactant molecules to the active sites.

The droplet is adsorbed completely on $Co(OH)_2$-CoP/MXene ultimately and the result manifests an exceptional hydrophilicity of the optimal catalyst. An initial CA is recorded and denoted as 20.43° when the droplet immediately contacted $Co(OH)_2$-CoP/MXene. The mounting evidences unearth the key role of P atom and MXene in constructing spin-cross interface of $Co(OH)_2$ and CoP, thus facilitating the adsorption

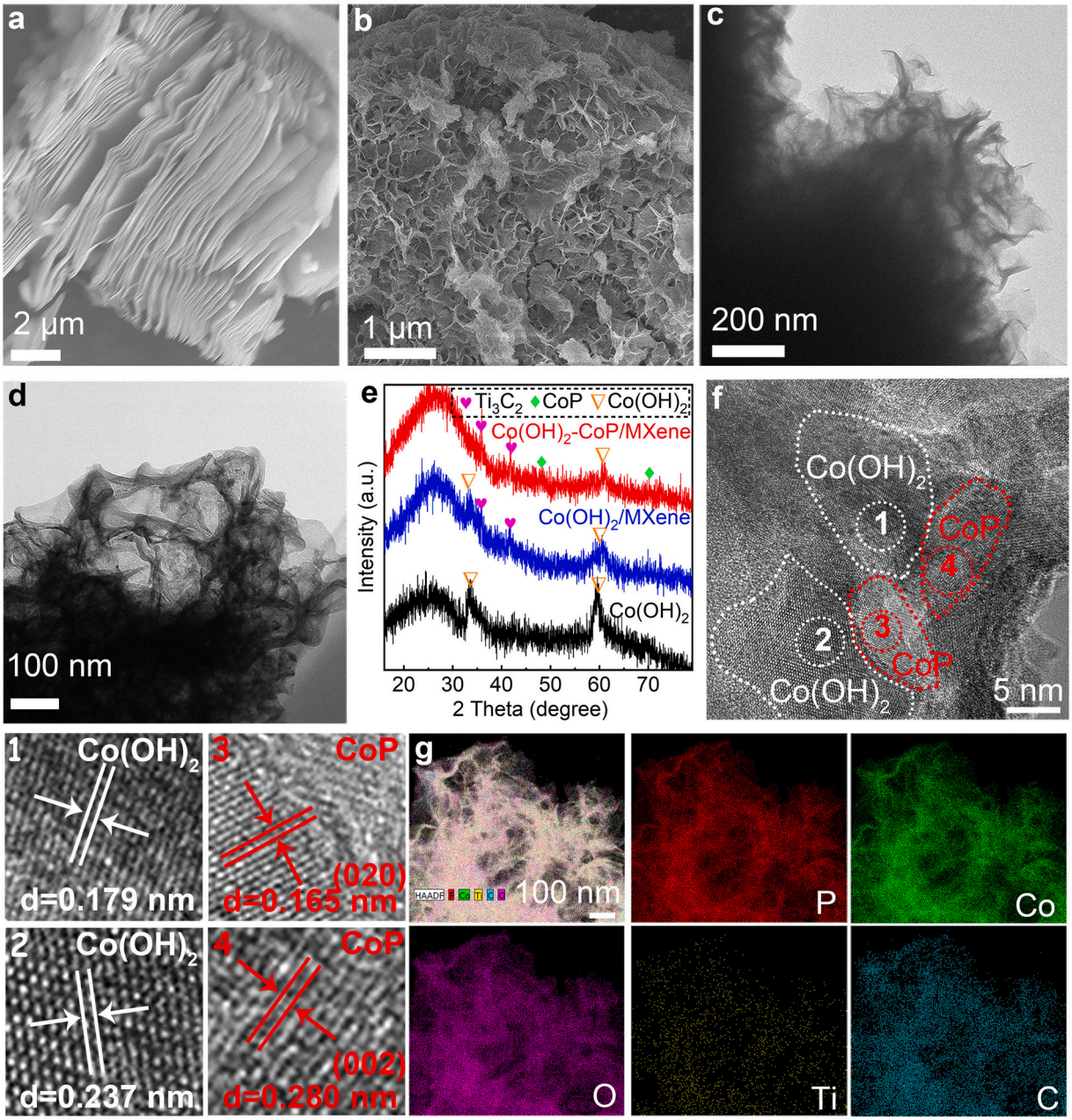

Fig. 3. SEM images of (a) MXene. (b, c) SEM and TEM images of $Co(OH)_2$/MXene. (d) TEM images of $Co(OH)_2$-CoP/MXene. (e) XRD patterns of various catalysts. (f) HRTEM images, (g) high-angle annular dark-field scanning transmission electron microscopy (HAADF-STEM) image and corresponding elemental mapping images of $Co(OH)_2$-CoP/MXene.

and activation of reactant molecules. Sequentially, the adsorption energies (E_{ad}) of NH_3BH_3 and H_2O molecules on various surfaces of catalysts are calculated by DFT. The corresponding E_{ad} of NH_3BH_3 (H_2O) on $Co(OH)_2$-CoP/MXene, $Co(OH)_2$-CoP, CoP and $Co(OH)_2$ is calculated by 1.642 (1.572 eV), 1.382 (1.323 eV), 0.715 (0.397 eV) and 0.459 (0.726 eV), respectively (Figs. 2d, 2e). The high values of E_{ad} interpret an easier adsorption of NH_3BH_3 and H_2O molecules on the surface of Co $(OH)_2$-CoP/MXene and facilitate the catalytic reaction.

The structural characterizations of various catalysts were clarified by SEM and TEM. In the SEM image in Fig. 3a, a layer structure MXene is observed. The $Co(OH)_2$/MXene is obtained after *in situ* hydroxylation reaction and the characteristic results confirm that $Co(OH)_2$ nanosheets have a perfect growth on MXene surface (Figs. 3b, 3c). The surface morphology of $Co(OH)_2$-CoP/MXene has no obvious change with Co $(OH)_2$-/MXene (Fig. 3d). The composition and structure of various catalysts were explored by X-ray diffraction (XRD). The peaks at 32.6° and 59.7° have perfect correspondence with $Co(OH)_2$ (JCPDS Card No. 74–1057) (Fig. 3e). The peaks at 35.9° and 41.7° are assigned to (111) and (200) planes of Ti_3C_2 (PDF No. 71–0298). Characteristic peaks at 48.2° and 70.2° are indexed to the (211) and (221) planes of CoP (PDF No. 29–0497). The broad peak between 20° and 30° is attributed to carbon. The characteristic peak of $Co(OH)_2$ is also detected in $Co(OH)_2$-CoP/MXene. The above XRD results expound that the successful construction of dual-active surfaces composed of $Co(OH)_2$ and CoP in Co $(OH)_2$-CoP/MXene. Notably, from the HRTEM image of $Co(OH)_2$-CoP/MXene in Fig. 3f, lattice fringes with lattice spacings of 0.179 nm and 0.237 nm are indexed to the (012) and (011) planes of $Co(OH)_2$ (PDF No. 74–1057). The lattice spacings of 0.165 nm and 0.280 nm are corresponding to the (020), (002) planes of CoP (PDF No. 29–0497). The above analysis illustrates that the successful construction of new interfacial $Co(OH)_xP_y$ with spin-cross interface of $Co(OH)_2$ and CoP. The HAADF-STEM coupling with the elemental mapping images uncover the uniform growth of $Co(OH)_2$ and CoP on the MXene nanosheets (Fig. 3g). The XRD patterns of contrast materials of CoP (black line), Co_3O_4 and

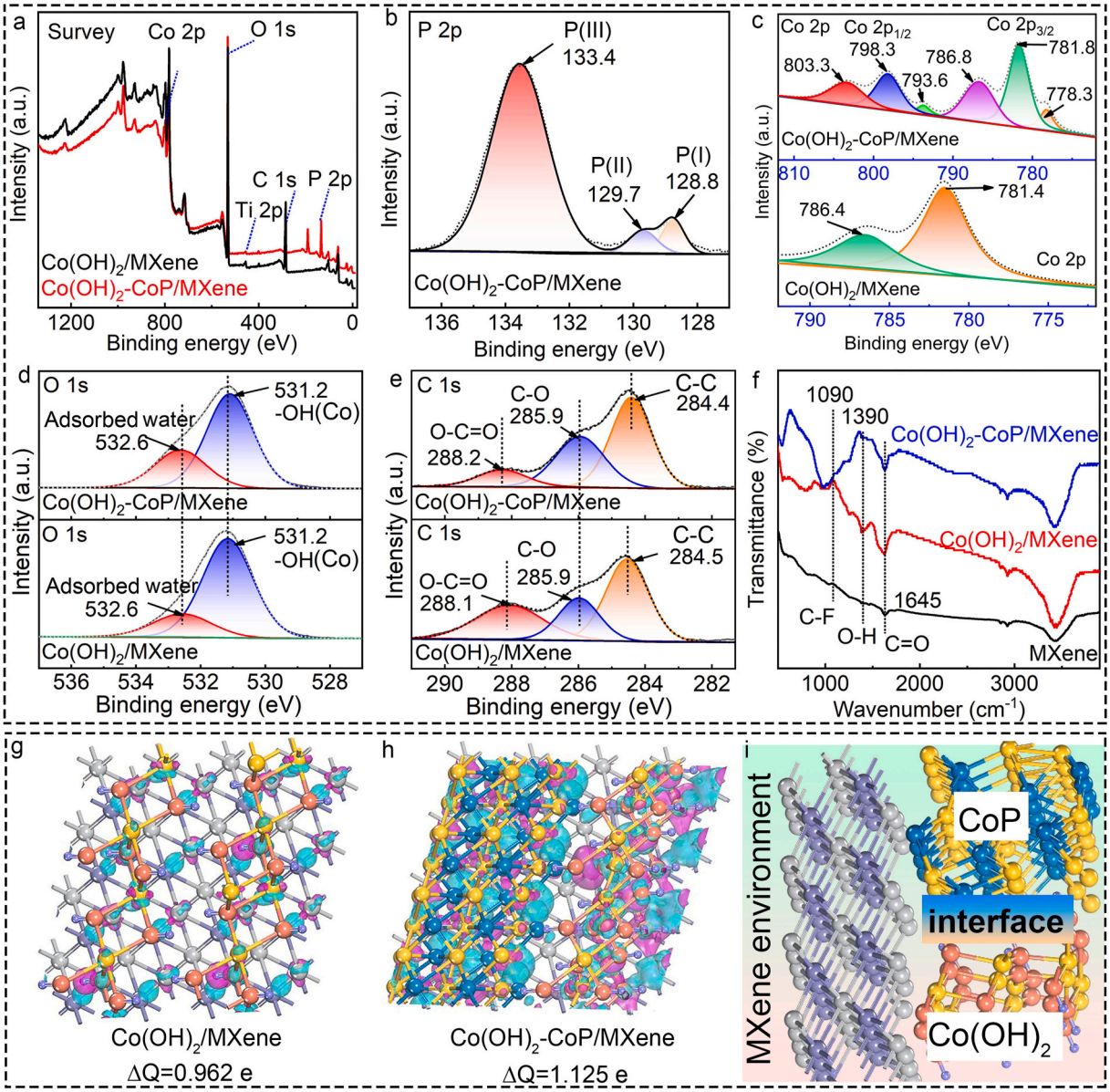

Fig. 4. Full spectra (a) and high-resolution XPS spectra of (b) P 2p, (c) Co 2p, (d) O 1 s, (e) C 1 s in $Co(OH)_2$/MXene, $Co(OH)_2$-CoP/MXene. (f) Fourier transform infrared spectroscopy of MXene, $Co(OH)_2$/MXene, $Co(OH)_2$-CoP/MXene. Atomic models and charge density difference of (g) $Co(OH)_2$/MXene and (h) $Co(OH)_2$-CoP/MXene with an iso-surface value of 0.03 eV·Å^{-3} (the cyan and yellow regions represent positive and negative charges, respectively). (i) The diagram of optimal structural model in this catalyst system.

Co_3O_4-P (blue line) derived from $Co(OH)_2$ (no MXene) are also performed. The characteristic peaks at 36.7°, 48.4° and 56.3° are corresponding to the (102), (202) and (212) planes of CoP. All the peaks at 31.3°, 36.8°, 44.8°, 59.4° and 65.2° in Co_3O_4 catalyst (green line) are perfectly matched with Co_3O_4 phase (JCPDS Card No. 42–1467) (Fig. S3). These results demonstrate that the presence of MXene has the ability to stabilize the $Co(OH)_2$ and provide the foundation for the further construction of the spin-cross interface of $Co(OH)_2$ and CoP.

The chemical composition and elemental states of various catalysts were determined by XPS. The survey spectra confirm that the elements of P, Co, O, Ti and C exist in $Co(OH)_2$-CoP/MXene (Fig. 4a). Three P species (P(I), P(II), and P(III)) at around 128.8 eV, 129.7 eV, and 133.4 eV in $Co(OH)_2$-CoP/MXene are observed in Fig. 4b [39,40]. This result exposes the successful fabrication of CoP. In Co 2p spectra of $Co(OH)_2$-CoP/MXene, the peaks at 778.3 eV (Co $2p_{3/2}$) and 793.6 eV (Co $2p_{1/2}$) are assigned to Co species in Co_xP [40]. Peaks at 781.8 eV (Co $2p_{3/2}$) and 798.3 eV (Co $2p_{1/2}$) are corresponding to Co^{2+} in $Co(OH)_2$ and/or oxidized Co species arising from superficial oxidation of Co_xP in air, respectively [41]. The peaks at 786.8 eV (Co $2p_{3/2}$) and 803.3 eV (Co $2p_{1/2}$) are ascribed to shake-up satellite peaks (Fig. 4c) [42,43]. In Co 2p spectra of $Co(OH)_2$/MXene, peaks at 781.4 (Co $2p_{3/2}$) and 786.4 eV (Co $2p_{1/2}$) are corresponding Co^{2+} in $Co(OH)_2$ (Fig. 4c) [44,45]. Compared with the binding energy of metallic Co (778.1 eV) and elemental phosphorus (130.0–130.2 eV), the binding energy of Co $2p_{3/2}$ has a positive shift and P $2p_{3/2}$ has a negative shift, respectively [44]. The result demonstrates an electron transfer from Co to P of Co $(OH)_2$-CoP/MXene because of the high electronegativity of P [46]. In the high resolution XPS spectra of O 1 s in $Co(OH)_2$-CoP/MXene and Co $(OH)_2$/MXene, peaks at 531.2 eV and 532.6 eV are indexed to -OH and adsorbed water, respectively (Fig. 4d) [47]. In the high resolution XPS spectra of C 1 s in $Co(OH)_2$-CoP/MXene and $Co(OH)_2$/MXene, peaks at 284.4/284.5 eV, 285.9 eV, 288.2/288.1 eV are ascribed to C−C, C−O, O−C=O, respectively (Fig. 4e) [32,48]. Additional elemental information from the XPS exposure in Table S1. Based on the HRTEM and the corresponding XPS analysis, the element P is successfully introduced into the $Co(OH)_2$-CoP/MXene. The FTIR spectrum for MXene, Co $(OH)_2$/MXene and $Co(OH)_2$-CoP/MXene are given in Fig. 4f. Experimentally, C–F (1090 cm^{-1}), O–H (1390 cm^{-1}) and C=O (1645 cm^{-1}) groups are observed [49]. Apparently, oxygen-containing functional groups appear on the surface of the catalyst. This oxygen-bound

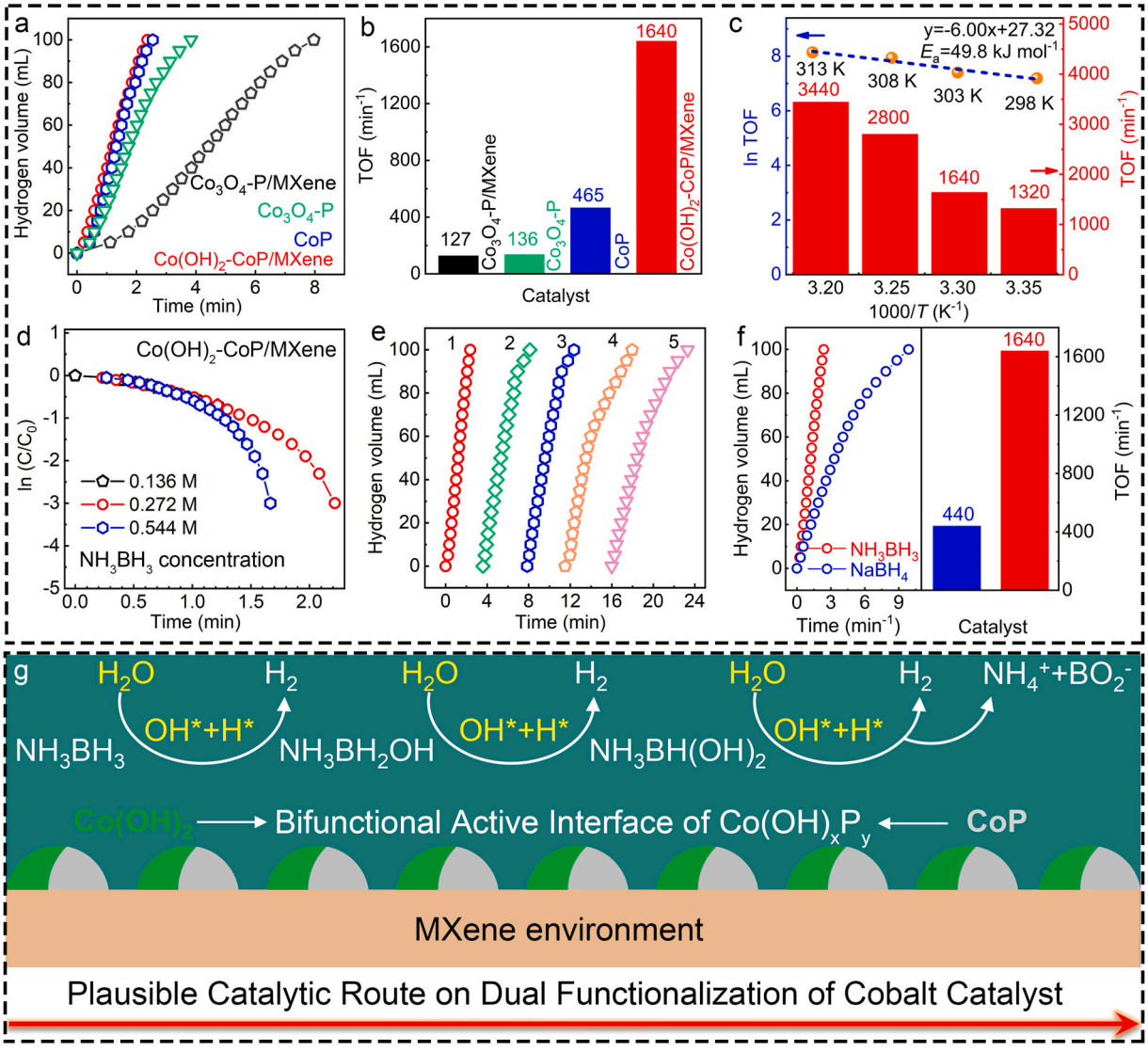

Fig. 5. (a, b) Hydrogen generation catalyzed by various catalysts and corresponding hydrogen generation activity (*TOF* min^{-1}). (c) Hydrogen generation of $Co(OH)_2$-CoP/MXene at different temperature and corresponding Arrhenius plot of ln (*TOF*) versus 1/*T*. (d) The corresponding curves of concentration changes *vs* time. Note: C refers to the real-time concentration; C_0 refers to the initial concentration. (e) Stability experiments of $Co(OH)_2$-CoP/MXene. (f) Hydrogen generation of $Co(OH)_2$-CoP/MXene for NH_3BH_3 and $NaBH_4$ and the corresponding *TOF*. (g) A plausible catalytic route for NH_3BH_3 hydrolysis over $Co(OH)_2$-CoP/MXene.

functional group is more active in forming synthetic hybrids through oxo-bridging, and exhibits improved catalytic performance [50]. To further intensively studied the interaction and charge transfer between the active component ($Co(OH)_2$-CoP) and MXene, the charge density difference of $Co(OH)_2$-CoP/MXene and $Co(OH)_2$/MXene is calculated and analyzed. Average Bader charge analysis demonstrates a charge transfer of 0.962 e from active component ($Co(OH)_2$) to MXene and a charge transfer of 1.125 e from active component ($Co(OH)_2$-CoP) to MXene after introducing P (Figs. 4g, 4h). The above results reveal that the construction of spin-cross interface in the intimate region between $Co(OH)_2$ and CoP leads to a significant charge redistribution. The enhanced metallic conductivity (MXene environments) and significant charge transfer of $Co(OH)_2$-CoP/MXene facilitates the catalytic reaction (Fig. 4i) [35].

3.3. Evaluation on catalytic kinetics

To investigate the catalytic kinetics of NH_3BH_3 hydrolysis, some operations are proceeded in this reaction system. The installation of hydrogen generation is referenced in previous work [51]. The contents of active component (Co elements) in Co_3O_4-P/MXene, Co_3O_4-P, CoP, $Co(OH)_2$-CoP/MXene catalysts are calculated as 42.23%, 62.02%, 37.63% and 28.72% by using ICP-OES technology, respectively (Table S2). And the corresponding dispersion degree values of Co on the surfaces are 7.89%, 10.31%, 6.23%, and 5.00%. Fig. 5a is the curve of hydrogen generation for NH_3BH_3 hydrolysis catalyzed by various catalysts. The calculated *TOF* of Co_3O_4-P/MXene, Co_3O_4-P, CoP, Co $(OH)_2$-CoP/MXene is 127, 136, 465, 1640 min^{-1}, respectively (Fig. 5b). The above results unambiguously unveiled that $Co(OH)_2$-CoP/MXene is the most optimal catalyst for this hydrolysis reaction. $Co(OH)_2$/MXene, $Co(OH)_2$, Co_3O_4 and Co_3O_4/MXene present poor catalytic activity (Fig. S4a).

Hydrogen generation experiments at different temperatures are researched to investigate the effect of temperature on the NH_3BH_3 hydrolysis (Fig. S4b). The *TOF* of $Co(OH)_2$-CoP/MXene significantly increased from 1320 min^{-1} at 298 K to 3440 min^{-1} at 313 K because of the fast transfer of reactant molecules (Fig. 5c). The calculation of the apparent activation energy (E_a) depends on the temperature from 298 to 313 K is determined by the Arrhenius Equation (Eq. S2) and the E_a of 49.8 $kJ{\cdot}mol^{-1}$ is deduced (Fig. 5c). The *TOF* and E_a of reported catalyst among TMPs or other supports in Table S3 comprehensively illustrate the top-ranked *TOF* of $Co(OH)_2$-CoP/MXene. Hydrogen generation of Co $(OH)_2$-CoP/MXene at different NH_3BH_3 concentrations are studied to certify the reaction kinetics and reaction order (Fig. S4c). These results verify that the catalyst has the flexibility in different working conditions and holds the promise in utilizing in industrial application. From the corresponding curves of NH_3BH_3 concentration changes *vs* time, a zero-order reaction is demonstrated in this reaction system (Fig. 5d). The hydrolysis of NH_3BH_3 at different mass concentration of catalyst is also conducted and results confirm that high mass concentration conveys an excellent catalytic activity because of the accumulation of effective active ingredient (Fig. S4d). In stability tests, the *TOF* of $Co(OH)_2$-CoP/MXene have no severe deactivation even after long-time usage (Fig. 5e).

The hydrogen generation on $Co(OH)_2$-CoP/MXene towards to $NaBH_4$ hydrolysis is explored under similar conditions to confirm the practicability of the catalyst for other borohydride. A corresponding *TOF* of 440 min^{-1} is obtained for the hydrolysis of $NaBH_4$ (Fig. 5 f). The negative catalytic activity is emerged for $NaBH_4$ compared to NH_3BH_3 (1640 min^{-1}). The reason is that the different catalytic mechanism between $NaBH_4$ and NH_3BH_3 hydrolysis caused by their different molecular geometry. The catalyst holds the promise and research space in catalyzing hydrolysis of $NaBH_4$ and exploring the corresponding catalytic mechanism. Series characterization analyses of the used $Co(OH)_2$-CoP/MXene are also conducted (Fig. S5). From the XRD pattern, the phase composition is resemble to the fresh $Co(OH)_2$-CoP/MXene (Fig. S5a). XPS analysis of the used $Co(OH)_2$-CoP/MXene proves the existence of P, Co, O, Ti and C elements, illustrating the excellent structure stability in this reaction system (Figs. S5b-5f). From the TEM images of the used $Co(OH)_2$-CoP/MXene, the morphologies of the catalyst remain moderate existential state with a little conglomeration (Figs. S5g-5j). The above results verify an excellent stability of the new structure of spin-cross interface in hydrolysis reaction. Fig. 5g presents the preliminary understanding about the mechanism of NH_3BH_3 hydrolysis takes place on the spin-cross interface. The existence of MXene is beneficial to stabilize $Co(OH)_2$ and make an attribution for the construction of spin-cross interface. The new structure of interfacial Co $(OH)_xP_y$ with bifunctional active interface alters the efficient adsorption and activation of NH_3BH_3 and H_2O molecules and ignites the catalytic activity for hydrogen generation.

3.4. Insights into catalytic mechanism

An analysis of *in situ* Raman spectra is given after broaching H_2O molecule onto catalysts. Two peaks at about 3240 and 3410 cm^{-1} are indexed to coordinated water. The results demonstrate the tendency of H_2O molecules to dissociation on the surfaces of catalysts (Fig. S6) [52]. The intensity of stretching of H_2O molecules on $Co(OH)_2$, $Co(OH)_2$/MXene and $Co(OH)_2$-CoP/MXene displays an growing tendency. The elucidation of *in situ* Raman spectroscopy intuitively demonstrated that more H_2O molecules adsorbed on $Co(OH)_2$-CoP/MXene surface than on other catalysts. The interaction between Co ion in $Co(OH)_2$ and H_2O molecule enhances the adsorption and dissociation of H_2O molecules. MXene plays a key role in stabilizing $Co(OH)_2$ and boosting the ability to adsorb H_2O molecules. The construction of spin-cross interface generated by *in situ* hydroxylation and P-inducing strategy promotes the ability of catalyst for the dissociation of H_2O molecules.

DFT calculations are adopted to elucidate the catalytic mechanistic regimes of spin-cross interface on $Co(OH)_2$-CoP/MXene toward NH_3BH_3 hydrolysis. Figs. 6a and 6b present the atomic structures of NH_3BH_3 and H_2O molecules on the surfaces of $Co(OH)_2$, CoP, $Co(OH)_2$-CoP, $Co(OH)_2$-CoP/MXene from the adsorption state to the transition state. The catalytic reaction is triggered by the adsorption of NH_3BH_3 and H_2O molecules on the surface of catalyst. Subsequently, the dissociation of NH_3BH_3 and H_2O molecules with the generation of H radical commences on the surface of catalyst. The Gibbs free energies corresponding to the transition states for NH_3BH_3 and H_2O dissociation on various surfaces of catalysts calculated by DFT simulation are provided (Figs. 6c, 6d). The reaction activation barriers (ΔE^*) obtained from the values of Gibbs free energies to substantiate the catalytic kinetics of catalysts. The ΔE^* of NH_3BH_3 molecule on $Co(OH)_2$-CoP/MXene (ΔE^*=0.488 eV) is lower than that on $Co(OH)_2$-CoP (ΔE^*=0.923 eV), CoP (ΔE=0.864 eV) and Co $(OH)_2$ (ΔE^*=1.308 eV) surfaces (Fig. 6e). Analogously, the ΔE^* of H_2O molecule on $Co(OH)_2$-CoP/MXene (ΔE^*=0.467 eV) conveys the optimal value compared with $Co(OH)_2$-CoP (ΔE^*=0.596 eV), CoP (ΔE^*=1.210 eV) and $Co(OH)_2$ (ΔE^*=0.622 eV) (Fig. 6 f). NH_3BH_3 and H_2O molecules exhibit the optimal dissociation kinetics on $Co(OH)_2$-CoP/MXene surface. The spin-cross interface of CoP and $Co(OH)_2$ in Co $(OH)_2$-CoP/MXene is responsible for the dissociation of NH_3BH_3 and H_2O molecules, respectively. The active site of Co-P in the spin-cross interface activates the NH_3BH_3 molecule and denoted as site 1. There are two types of active sites exist in the dissociation of H_2O molecule on $Co(OH)_2$ active surface: (1) The hydroxyl in $Co(OH)_2$ is the active site. Namely, the O atom (H atom) in hydroxyl combines with the H atom (O atom) in H_2O to form a hydrogen bond to boost the dissociation of the H_2O molecule. (2) The cobalt ion in $Co(OH)_2$ is the active site. In detail, the coordination between the cobalt ion in $Co(OH)_2$ and the O atom in H_2O forms the active site to activate the H_2O molecule. The activation of H_2O molecule on $Co(OH)_2$ surface is the compatible integration of the above-mentioned process because of the complexity of practical heterogeneous catalysis. And the above active site is denoted as site 2. Fig. 6 g depicts the dissociation-interaction mechanism of spin-cross interface in $Co(OH)_xP_y$ on the surface of MXene. The simulated

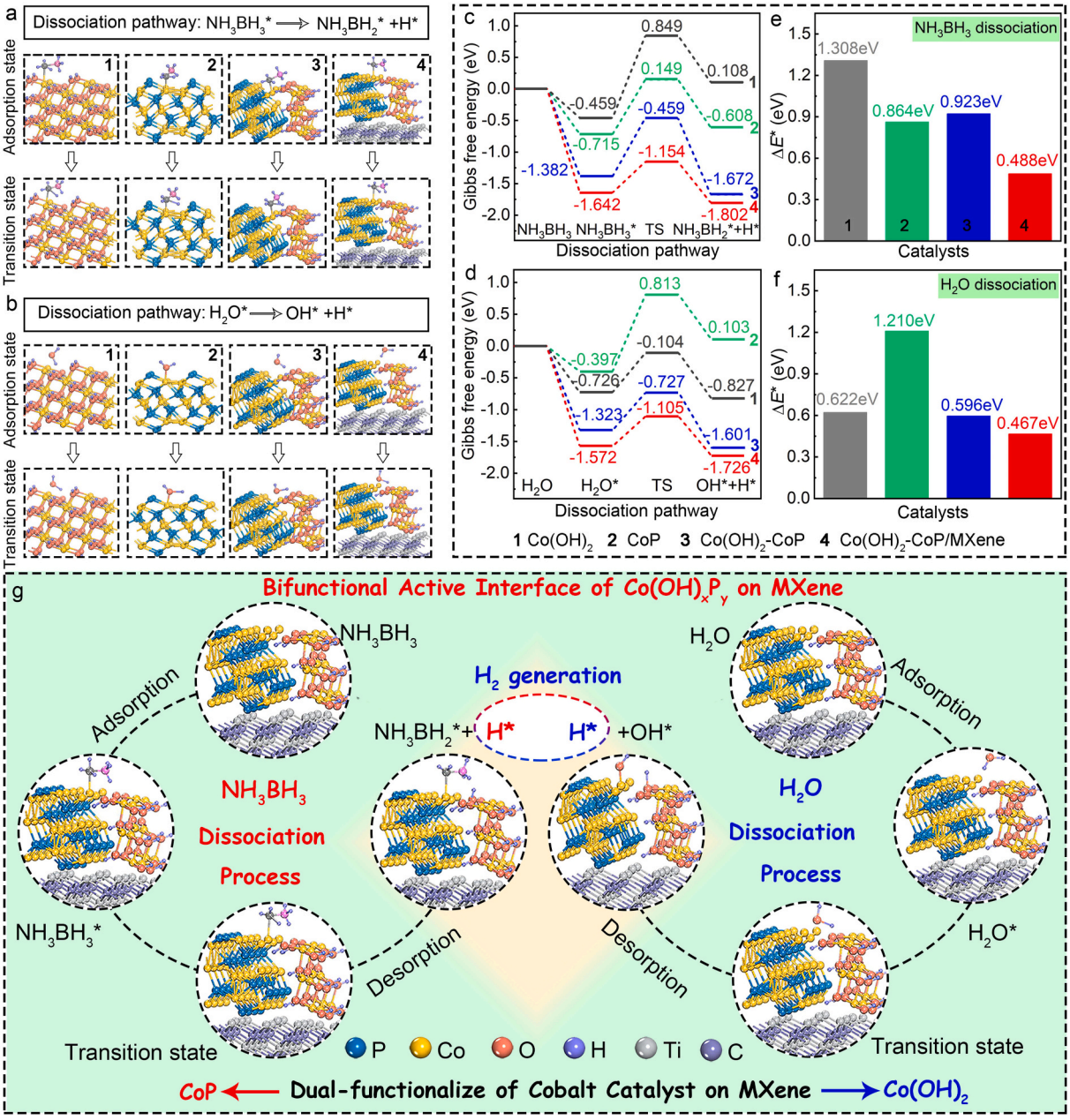

Fig. 6. (a, b) The optimized atomic structural models from the adsorption state to the transition state, (c, d) the Gibbs free energy and (e, f) the ΔE^* for the dissociation of NH_3BH_3 and H_2O molecule on various surfaces. (g) Proposed theoretical reflections on catalytic mechanism of $Co(OH)_2$-CoP/MXene for NH_3BH_3 hydrolysis.

pathways are proposed as follows,

NH_3BH_3+2[site 1]*→NH_3BH_2-[site 1]*+H-[site 1]* (1-1)

H_2O+2[site 2]*→H-[site 2]*+OH-[site 2]* (1-2)

H-[site 1]*+H-[site 2]*→H_2+[site 1]*+[site 2]* (1-3)

NH_3BH_2-[site 1]*+OH-[site 2]*→NH_3BH_2OH-[site 1]*+[site 2]* (1-4)

NH_3BH_2OH-[site 1]*+[site 1]*→NH_3BHOH-[site 1]*+H-[site 1]* (1-5)

H-[site 1]*+H-[site 2]*→H_2+[site 1]*+[site 2]* (1-6)

NH_3BHOH-[site 1]*+OH-[site 2]*→$NH_3BH(OH)_2$-[site 1]*+[site 2]* (1-7)

$NH_3BH(OH)_2$-[site 1]*→NH_3BHO-[site 1]*+H_2O (1-8)

NH_3BHO-[site 1]*+[site 1]*+OH-[site 2]*→NH_3BOOH-[site 1]*+H-[site 1]*+[site 2]* (1-9)

H-[site 1]*+H-[site 2]*→H_2+[site 1]*+[site 2]* (1-10)

NH_3BOOH-[site 1]*→NH_4^++BO_2^-+[site 1]* (1-11)

In the initial stage, NH_3BH_3, H_2O and $Co(OH)_2$-CoP/MXene are both independent states. NH_3BH_3 and H_2O molecules are adsorbed on the surface of catalyst through the activation by site 1 and site 2 form NH_3BH_3-[site 1]* and H_2O-[site 1]*, respectively. The B–H bond in NH_3BH_3-[site 1]* break to form NH_3BH_2-[site 1]* and H-[site 1]*. The O–H bond in H_2O-[site 2]* break to form OH-[site 2]* and H-[site 2]*. Subsequently, H-[site 1]* and H-[site 2]* generate a H_2 molecule to be released from the surface of catalyst. The remaining OH-[site 2]* combines with NH_3BH_2-[site 1]* form NH_3BH_2OH*. Coincidentally, the reaction intermediate of NH_3BH_2OH* becomes the initial state for the

further reaction until the other two H_2 molecules are released (Fig. 6e). The above analyses propose that the interface between $Co(OH)_2$ and CoP on the surface of MXene present abundant active sites. The bifunctional interfacial $Co(OH)_xP_y$ sites express efficient catalytic activity toward hydrogen generation. It is reasonable to consider the interactions between the NH_3BH_3 molecule and the surface of active component to form complex species via the oxidation addition and reductive elimination [53–55].

A plausible catalytic mechanism on oxidation addition of O–H and reductive eliminate of H_2 during NH_3BH_3 hydrolysis is investigated (from Eq.1–1 to Eq. 1–11). A hydride transfer of B–H bond for NH_3BH_3 is occurred. Subsequently, the hydridic surface has the beneficial to close the acidic H atom in H_2O through electrostatic interaction. The dissociation of O–H bond in H_2O and B–H bond in NH_3BH_3 forms M-H bonds on the catalyst surface through an oxidative addition. Then, the generation of H_2 releases from the surface of catalyst through a reductive elimination. This hypothesis provides further theoretical direction for the catalytic mechanism of NH_3BH_3 hydrolysis. Actually, the above-related mechanism is consistent with the mechanism proposed in this research. The difference is that the reaction molecules begin to react under the status of incomplete dissociation in the mechanism of oxidation addition and reductive elimination. Illustratively, the catalytic mechanisms depend on specific catalysts. Thus, the confirmation of rate-determining step (oxidative addition or reductive elimination) is the key scientific challenge in the hydrogen generation from NH_3BH_3. The formation of ring-mounted intermediate is the possible step following the oxidation addition during NH_3BH_3 hydrolysis. The above insights into the catalytic mechanism provides effective theoretical guidance.

4. Conclusions

In conclusion, a spin-cross interface in the intimate region between $Co(OH)_2$ and CoP on MXene constructed by *in situ* hydroxylation and P-inducing strategy is demonstrated to be effective for boosting the catalytic activity towards hydrogen generation. The optimal catalyst displays outstanding catalytic kinetics with an unprecedented *TOF* of 1640 min^{-1}. This *TOF* value is at the first level among the non-noble metal-based catalysts in alkali-free hydrolysis of NH_3BH_3. The construction of $Co(OH)_xP_y$ active sites with spin-cross interface boosts the intrinsic catalytic activity of $Co(OH)_2$-CoP/MXene. The bifunctional active sites deriving from the intimate region between $Co(OH)_2$ and CoP is responsible for the dissociation of reactant molecules ($Co(OH)_2$ side activates H_2O, CoP side activates NH_3BH_3). Experimental and theoretical results substantiate that the reducing energy barrier for dissociation of reactant molecules on spin-cross interface promotes the catalytic activity toward hydrogen generation. This research exploits an avenue to increasing the catalytic efficiency by constructing MXene-based spin-cross interface in catalysts.

CRediT authorship contribution statement

Jianchun Jiang: Visualization, Formal analysis. **Xianli Wu:** Formal analysis. **Xianji Guo:** Formal analysis. **Lixia Wang:** Formal analysis. **Baojun Li:** Visualization, Validation, Project administration, Investigation, Funding acquisition, Formal analysis, Conceptualization. **Yongfeng Wang:** Visualization, Supervision, Project administration, Investigation, Formal analysis. **Baozhong Liu:** Visualization, Supervision, Project administration, Formal analysis. **Jingjing Zhou:** Formal analysis. **Huanhuan Zhang:** Writing – review & editing, Writing – original draft, Software, Formal analysis, Data curation. **Yanyan Liu:** Validation, Project administration, Investigation, Formal analysis, Conceptualization. **Xia Sheng:** Formal analysis. **Wenbo Zhang:** Formal analysis. **Ruofan Shen:** Formal analysis. **Shuyan Guan:** Formal analysis.

Declaration of Competing Interest

The authors declare that they have no known competing financial interests or personal relationships that could have appeared to influence the work reported in this paper.

Data availability

Data will be made available on request.

Acknowledgments

Financial supports from the Young Top Talent Program of Zhongyuan-Yingcai-Jihua (No. 30602674), the Top-Notch Talent Program of Henan Agricultural University (No. 30501034), the National Natural Science Foundation of China (Nos. 22279118, 22279117, 22075254, U22A20120, 52071135), and the National Science Fund for Distinguished Young of China (No. 22225202) are acknowledged. Experiments were supported by Peking Nanofab. All authors thank the Communist Party of China.

Appendix A. Supporting information

Supplementary data associated with this article can be found in the online version at doi:10.1016/j.apcatb.2024.124143.

References

[1] C.-C. Hou, Q. Li, C.-J. Wang, C.-Y. Peng, Q.-Q. Chen, H.-F. Ye, W.-F. Fu, C.-M. Che, N. López, Y. Chen, Ternary Ni–Co–P nanoparticles as noble-metal-free catalysts to boost the hydrolytic dehydrogenation of ammonia-borane, Energy Environ. Sci. 10 (2017) 1770–1776.
[2] R. Shen, Y. Liu, H. Zhang, S. Liu, H. Wei, H. Yuan, H. Wen, X. Wu, S. Mehdi, T. Liu, J. Jiang, E. Liang, B. Li, Coupling oxygen vacancy and hetero-phase junction for boosting catalytic activity of Pd toward hydrogen generation, Appl. Catal. B Environ. 328 (2023) 122484.
[3] S.-J. Li, H.-L. Wang, B.-R. Wulan, X. Zhang, J.-M. Yan, Q. Jiang, Complete dehydrogenation of $N_2H_4BH_3$ over noble-metal-free $Ni_{0.5}Fe_{0.5}$–CeO_x/MIL-101 with high activity and 100% H_2 selectivity, Adv. Energy Mater. 8 (2018) 1800625.
[4] Z.-P. Wu, X.F. Lu, S.-Q. Zang, X.W. (David) Lou, Non-noble-metal-based electrocatalysts toward the oxygen evolution reaction, Adv. Funct. Mater. 30 (2020) 1910274.
[5] C.Y. Zhang, C. Zhang, G.W. Sun, J.L. Pan, L. Gong, G.Z. Sun, J.J. Biendicho, L. Balcells, X.L. Fan, J.R. Morante, J.Y. Zhou, A. Cabot, Spin effect to promote reaction kinetics and overall performance of lithium-sulfur batteries under external magnetic field, Angew. Chem. Int. Ed. 61 (2022) e202211570.
[6] M. Li, S. Zhang, J. Zhao, H. Wang, Maximizing metal–support interactions in Pt/Co_3O_4 nanocages to simultaneously boost hydrogen production activity and durability, ACS Appl. Mater. Interfaces 13 (2021) 57362–57371.
[7] W.-W. Zhan, Q.-L. Zhu, Q. Xu, Dehydrogenation of ammonia borane by metal nanoparticle catalysts, ACS Catal. 6 (2016) 6892–6905.
[8] Z. Li, Z. Wang, S. Xi, X. Zhao, T. Sun, J. Li, W. Yu, H. Xu, T.S. Herng, X. Hai, P. Lyu, M. Zhao, S.J. Pennycook, J. Ding, H. Xiao, J. Lu, Tuning the spin density of cobalt single-atom catalysts for efficient oxygen evolution, ACS Nano 15 (2021) 7105–7113.
[9] G. Yang, J. Zhu, P. Yuan, Y. Hu, G. Qu, B.-A. Lu, X. Xue, H. Yin, W. Cheng, J. Cheng, W. Xu, J. Li, J. Hu, S. Mu, J.-N. Zhang, Regulating Fe-spin state by atomically dispersed Mn-N in Fe-N-C catalysts with high oxygen reduction activity, Nat. Commun. 12 (2021) 1734.
[10] K. Liu, R. Qin, N. Zheng, Insights into the interfacial effects in heterogeneous metal nanocatalysts toward selective hydrogenation, J. Am. Chem. Soc. 143 (2021) 4483–4499.
[11] L. Zhang, M. Zhou, A. Wang, T. Zhang, Selective hydrogenation over supported metal catalysts: from nanoparticles to single atoms, Chem. Rev. 120 (2020) 683–733.
[12] T.W. van Deelen, C. Hernández Mejía, K.P. de Jong, Control of metal-support interactions in heterogeneous catalysts to enhance activity and selectivity, Nat. Catal. 2 (2019) 955–970.
[13] H. Zhou, T. Liu, X. Zhao, Y. Zhao, H. Lv, S. Fang, X. Wang, F. Zhou, Q. Xu, J. Xu, C. Xiong, Z. Xue, K. Wang, W. Cheong, W. Xi, L. Gu, T. Yao, S. Wei, X. Hong, J. Luo, Y. Li, Y. Wu, A supported nickel catalyst stabilized by a surface digging effect for efficient methane oxidation, Angew. Chem. Int. Ed. 58 (2019) 18388–18393.
[14] D. Guo, F. Ming, D.B. Shinde, L. Cao, G. Huang, C. Li, Z. Li, Y. Yuan, M.N. Hedhili, H.N. Alshareef, Z. Lai, Covalent assembly of two-dimensional COF-on-MXene heterostructures enables fast charging lithium hosts, Adv. Funct. Mater. 31 (2021) 2101194.

[15] H. Zhang, Z. Wei, J. Wu, F. Cheng, Y. Ma, W. Liu, Y. Cheng, Y. Lin, N. Liu, Y. Gao, Y. Yue, Interlayer-spacing-regulated MXene/rGO foam for multi-functional zinc-ion microcapacitors, Energy Storage Mater. 50 (2022) 444–453.
[16] Y. Long, Y. Tao, T. Shang, H. Yang, Z. Sun, W. Chen, Q. Yang, Roles of metal ions in MXene synthesis, processing and applications: a perspective, Adv. Sci. 9 (2022) 2200296.
[17] H.-Y. Wang, X.-B. Sun, S.-H. Yang, P.-Y. Zhao, X.-J. Zhang, G.-S. Wang, Y. Huang, 3D Ultralight hollow NiCo compound@MXene composites for tunable and high-efficient microwave absorption, Nano-Micro Lett. 13 (2021) 206.
[18] H. Zhang, K. Zhang, S. Ashraf, Y. Fan, S. Guan, X. Wu, Y. Liu, B. Liu, B. Li, Polar O–Co–P surface for bimolecular activation in catalytic hydrogen generation, Energy Environ. Mater. 6 (2023) e12273.
[19] S. Mehdi, Y. Liu, H. Wei, H. Zhang, R. Shen, S. Guan, X. Wu, T. Liu, H. Wen, Z. Peng, C. Wang, Z. Liu, H. Cao, B. Li, P-induced Co-based interfacial catalysis on Ni foam for hydrogen generation from ammonia borane, Appl. Catal. B Environ. 325 (2023) 122317.
[20] Y. Liu, G. Han, X. Zhang, C. Xing, C. Du, H. Cao, B. Li, Co-Co_3O_4@carbon core–shells derived from metal−organic framework nanocrystals as efficient hydrogen evolution catalysts, Nano Res 10 (2017) 3035–3048.
[21] Y. Zhong, I. Douair, T. Wang, C. Wu, L. Maron, D. Cui, Access to hydroxy-functionalized polypropylene through coordination polymerization, Angew. Chem. Int. Ed. 59 (2020) 4947–4952.
[22] Y. Liu, X. Liu, X. Wang, H. Ning, T. Yang, J. Yu, A. Kumar, Y. Luo, H. Wang, L. Wang, J. Lee, A.R. Jadhav, H. Hu, M. Wu, M.G. Kim, H. Lee, Unraveling the synergy of chemical hydroxylation and the physical heterointerface upon improving the hydrogen evolution kinetics, ACS Nano 15 (2021) 15017–15026.
[23] W. Deng, L. Zhang, L. Li, S. Chen, C. Hu, Z.-J. Zhao, T. Wang, J. Gong, Crucial role of surface hydroxyls on the activity and stability in electrochemical CO_2 reduction, J. Am. Chem. Soc. 141 (2019) 2911–2915.
[24] B. Liu, B. Zhang, J. Ji, K. Li, J. Cao, Q. Feng, H. Huang, Effective regulation of surface bridging hydroxyls on TiO_2 for superior photocatalytic activity via ozone treatment, Appl. Catal. B Environ. 304 (2022) 120952.
[25] D. Zhang, P. Ren, W. Liu, Y. Li, S. Salli, F. Han, W. Qiao, Y. Liu, Y. Fan, Y. Cui, Y. Shen, E. Richards, X. Wen, M.H. Rummeli, Y. Li, F. Besenbacher, H. Niemantsverdriet, T. Lim, R. Su, Photocatalytic abstraction of hydrogen atoms from water using hydroxylated graphitic carbon nitride for hydrogenative coupling reactions, Angew. Chem. Int. Ed. 61 (2022) e202204256.
[26] Y. Zhou, H. Liu, X. Gu, X. Wu, L. Feng, Hetero MOF-on-MOF-derived carbon nanotube interconnected nitrogen-doped carbon-encapsulated FeNi/FeF_2 for efficient oxygen evolution reaction, Carbon Energy 4 (2022) 924–938.
[27] P. Zhang, X.F. Lu, J. Nai, S. Zang, X.W. (David) Lou, Construction of hierarchical Co–Fe oxyphosphide microtubes for electrocatalytic overall water splitting, Adv. Sci. 6 (2019) 1900576.
[28] J. Mei, J. Shang, T. He, D. Qi, L. Kou, T. Liao, A. Du, Z. Sun, 2D/2D black phosphorus/nickel hydroxide heterostructures for promoting oxygen evolution via electronic structure modulation and surface reconstruction, Adv. Energy Mater. 12 (2022) 2201141.
[29] W. Liu, H. Gao, Z. Zhang, Y. Zheng, Y. Wu, X. Fu, J. Su, Y. Gao, CoP/Cu_3P heterostructured nanoplates for high-rate supercapacitor electrodes, Chem. Eng. J. 437 (2022) 135352.
[30] Y.-J. Tang, Y. Zou, D. Zhu, Efficient water oxidation using an Fe-doped nickel telluride–nickel phosphide electrocatalyst by partial phosphating, J. Mater. Chem. A 10 (2022) 12438–12446.
[31] H. Yan, C. Tian, L. Wang, A. Wu, M. Meng, L. Zhao, H. Fu, Phosphorus-modified tungsten nitride/reduced graphene oxide as a high-performance, non-noble-metal electrocatalyst for the hydrogen evolution reaction, Angew. Chem. Int. Ed. 54 (2015) 6325–6329.
[32] F. Yao, S. Guan, L. Bian, Y. Fan, X. Liu, H. Zhang, B. Li, B. Liu, Ensemble-exciting effect in Pd/alk-Ti_3C_2 on the activity for efficient hydrogen production, ACS Sustain. Chem. Eng. 9 (2021) 12332–12340.
[33] X. Yang, Q. Li, L. Li, J. Lin, X. Yang, C. Yu, Z. Liu, Y. Fang, Y. Huang, C. Tang, CuCo binary metal nanoparticles supported on boron nitride nanofibers as highly efficient catalysts for hydrogen generation from hydrolysis of ammonia borane, J. Power Sources 431 (2019) 135–143.
[34] Y. Chen, J. Cai, P. Li, G. Zhao, G. Wang, Y. Jiang, J. Chen, S.X. Dou, H. Pan, W. Sun, Hexagonal boron nitride as a multifunctional support for engineering efficient electrocatalysts toward the oxygen reduction reaction, Nano Lett. 20 (2020) 6807–6814.
[35] Q. Peng, J. Zhou, J. Chen, T. Zhang, Z. Sun, Cu single atoms on Ti_2CO_2 as a highly efficient oxygen reduction catalyst in a proton exchange membrane fuel cell, J. Mater. Chem. A 7 (2019) 26062–26070.
[36] D. Guo, X. Li, Y. Jiao, H. Yan, A. Wu, G. Yang, Y. Wang, C. Tian, H. Fu, A dual-active Co-CoO heterojunction coupled with Ti_3C_2-MXene for highly-performance overall water splitting, Nano Res 15 (2022) 238–247.
[37] A. Kumar, V.Q. Bui, J. Lee, A.R. Jadhav, Y. Hwang, M.G. Kim, Y. Kawazoe, H. Lee, Modulating interfacial charge density of NiP_2–FeP_2 via coupling with metallic Cu for accelerating alkaline hydrogen evolution, ACS Energy Lett. 6 (2021) 354–363.
[38] X. Ji, Y. Lin, J. Zeng, Z. Ren, Z. Lin, Y. Mu, Y. Qiu, J. Yu, Graphene/MoS_2/FeCoNi$(OH)_x$ and Graphene/MoS_2/FeCoNiP_x multilayer-stacked vertical nanosheets on carbon fibers for highly efficient overall water splitting, Nat. Commun. 12 (2021) 1380.
[39] T. Wang, Y. Jiang, Y. Zhou, Y. Du, C. Wang, In situ electrodeposition of CoP nanoparticles on carbon nanomaterial doped polyphenylene sulfide flexible electrode for electrochemical hydrogen evolution, Appl. Surf. Sci. 442 (2018) 1–11.
[40] Y. Zhao, X. Wang, G. Cheng, W. Luo, Phosphorus-induced activation of ruthenium for boosting hydrogen oxidation and evolution electrocatalysis, ACS Catal. 10 (2020) 11751–11757.
[41] G. Huang, L. Zhao, S. Yuan, N. Li, S. Jing, Iron doped mesoporous cobalt phosphide with optimized electronic structure for enhanced hydrogen evolution, Int. J. Hydrog. Energy 47 (2022) 14767–14776.
[42] J. Guo, B. Wang, D. Yang, Z. Wan, P. Yan, J. Tian, T.T. Isimjan, X. Yang, Rugae-like Ni_2P-CoP nanoarrays as a bi-functional catalyst for hydrogen generation: $NaBH_4$ hydrolysis and water reduction, Appl. Catal. B Environ. 265 (2020) 118584.
[43] L. Zhang, G. Wang, X. Hao, Z. Jin, Y. Wang, MOFs-derived Cu_3P@CoP p-n heterojunction for enhanced photocatalytic hydrogen evolution, Chem. Engi. J. 395 (2020) 125113.
[44] M. Chen, H. Li, C. Wu, Y. Liang, J. Qi, J. Li, E. Shangguan, W. Zhang, R. Cao, Interfacial engineering of heterostructured $Co(OH)_2$/NiP_x nanosheets for enhanced oxygen evolution reaction, Adv. Funct. Mater. 32 (2022) 2206407.
[45] Y. Pan, K. Sun, S. Liu, X. Cao, K. Wu, W.-C. Cheong, Z. Chen, Y. Wang, Y. Li, Y. Liu, D. Wang, Q. Peng, C. Chen, Y. Li, Core–shell ZIF-8@ZIF-67-derived CoP nanoparticle-embedded N-doped carbon nanotube hollow polyhedron for efficient overall water splitting, J. Am. Chem. Soc. 140 (2018) 2610–2618.
[46] J. Tian, Q. Liu, A.M. Asiri, X. Sun, Self-supported nanoporous cobalt phosphide nanowire arrays: an efficient 3D hydrogen-evolving cathode over the wide range of pH 0–14, J. Am. Chem. Soc. 136 (2014) 7587–7590.
[47] M. Fan, J.D. Jimenez, S.N. Shirodkar, J. Wu, S. Chen, L. Song, M.M. Royko, J. Zhang, H. Guo, J. Cui, K. Zuo, W. Wang, C. Zhang, F. Yuan, R. Vajtai, J. Qian, J. Yang, B.I. Yakobson, J.M. Tour, J. Lauterbach, D. Sun, P.M. Ajayan, Atomic Ru immobilized on porous h-BN through simple vacuum filtration for highly active and selective CO_2 methanation, ACS Catal. 9 (2019) 10077–10086.
[48] Y.-Z. Fang, R. Hu, K. Zhu, K. Ye, J. Yan, G. Wang, D. Cao, Aggregation-resistant 3D $Ti_3C_2T_x$ MXene with enhanced kinetics for potassium ion hybrid capacitors, Adv. Funct. Mater. 30 (2020) 2005663.
[49] P. Yan, R. Zhang, J. Jia, C. Wu, A. Zhou, J. Xu, X. Zhang, Enhanced supercapacitive performance of delaminated two-dimensional titanium carbide/carbon nanotube composites in alkaline electrolyte, J. Power Sources 284 (2015) 38–43.
[50] J. Li, X. Yuan, C. Lin, Y. Yang, L. Xu, X. Du, J. Xie, J. Lin, J. Sun, Achieving high pseudocapacitance of 2D titanium carbide (MXene) by cation intercalation and surface modification, Adv. Energy Mater. 7 (2017) 1602725.
[51] W. Xu, W. Li, H. Wen, J. Ding, Y. Liu, W. Li, B. Li, Metal/metal-organic framework interfacial ensemble-induced dual site catalysis towards hydrogen generation, Appl. Catal. B Environ. 286 (2021) 119946.
[52] R. Shen, Y. Liu, H. Wen, X. Wu, G. Han, X. Yue, S. Mehdi, T. Liu, H. Cao, E. Liang, B. Li, Engineering bimodal oxygen vacancies and Pt to boost the activity toward water dissociation, Small 18 (2022) 2105588.
[53] A. Bismuto, T. Delcaillau, P. Müller, B. Morandi, Nickel-catalyzed amination of aryl thioethers: a combined synthetic and mechanistic study, ACS Catal. 10 (2020) 4630–4639.
[54] S. Gisbertz, S. Reischauer, B. Pieber, Overcoming limitations in dual photoredox/nickel-catalysed C–N cross-couplings due to catalyst deactivation, Nat. Catal. 3 (2020) 611–620.
[55] Q. Xu, M. Chandra, Catalytic activities of non-noble metals for hydrogen generation from aqueous ammonia–borane at room temperature, J. Power Sources 163 (2006) 364–370.